Toward the global fit of the TMD gluon density in the proton from the LHC data

A. V. Lipatov,[1,2] G. I. Lykasov,[2] and M. A. Malyshev[1,2]

[1]*Skobeltsyn Institute of Nuclear Physics, Lomonosov Moscow State University, 119991, Moscow, Russia*
[2]*Joint Institute for Nuclear Research, 141980, Dubna, Moscow region, Russia*

(Received 8 November 2022; accepted 19 December 2022; published 23 January 2023)

We propose a new analytical expression for the transverse-momentum-dependent (TMD, or unintegrated) gluon density in the proton. Essential phenomenological parameters are extracted from the LHC data on inclusive hadron production in pp collisions at low transverse momenta $p_T \leq 1$ GeV. The latter are described in the framework of a modified soft quark-gluon string model, where the gluonic state and nonzero transverse momentum of partons inside the proton are taken into account. To determine the parameters important at moderate and large x, we use the measurements of inclusive b-jet and Higgs boson production at the LHC as well as the latest HERA data on proton structure functions $F_2^c(x, Q^2)$ and $F_2^b(x, Q^2)$ and reduced cross sections $\sigma_{\rm red}^c(x, Q^2)$ and $\sigma_{\rm red}^b(x, Q^2)$. The Catani-Ciafaloni-Fiorani-Marchesini evolution equation is applied to extend the initial gluon distribution to the whole kinematical region. We achieve a simultaneous description of all considered processes with $\chi^2/\text{d.o.f.} = 2.2$, thus moving toward the global fit of the TMD gluon density from collider data. The obtained TMD gluon distribution in a proton is available for public usage and implemented in the TMDLIB package and Monte Carlo event generator PEGASUS.

DOI: 10.1103/PhysRevD.107.014022

I. INTRODUCTION

It is known that the theoretical description of any physical observables measured in the collider experiments is mainly based on different factorization theorems in quantum chromodynamics (QCD). These theorems provide the necessary framework to separate hard partonic physics, described with the perturbative QCD expansion, from soft hadronic physics, described in terms of parton density functions (PDFs). The latter contain information on the nonperturbative structure of a hadron (proton). The most popular framework is provided by the conventional (so-called collinear) QCD factorization. In this approach, gluon and quark densities depend only on the longitudinal momentum fraction x of the proton momentum carried by a parton. An appropriate QCD evolution describing the dependence of PDFs on the resolution scale μ^2 is given by the Dokshitzer-Gribov-Lipatov-Altarelli-Parisi (DGLAP) equations [1]. Such a formalism is usually successful for sufficiently inclusive processes, like deep-inelastic lepton-hadron scattering (DIS), if a few higher-order terms in perturbative QCD expansion are taken into account. However, in order to describe less inclusive processes proceeding at high energies with large momentum transfer and/or containing multiple hard scales, the transverse-momentum-dependent (TMD, or unintegrated) parton densities $f_a(x, \mathbf{k}_T^2, \mu^2)$ with $a = q$ or g are required (for more information, see, for example, Ref. [2] and references therein). These quantities encode additional transverse momentum and polarization degrees of freedom and satisfy the Balitsky-Fadin-Kuraev-Lipatov (BFKL) [3] or Catani-Ciafaloni-Fiorani-Marchesini (CCFM) [4] evolution equations. In this way, one can effectively resum large logarithmic terms proportional to $\alpha_s^n \ln^n s/\Lambda_{\rm QCD}^2 \sim \alpha_s^n \ln^n 1/x$ which are expected to become equally (or even more) important in comparison with conventional DGLAP contributions proportional to $\alpha_s^n \ln^n \mu^2/\Lambda_{\rm QCD}^2$. Such a high-energy factorization [5], or k_T-factorization [6] formalism, was formulated and it is becoming a widely exploited tool in high-energy physics. A certain advantage of this approach is that one can quite easily take into account a large piece of higher-order perturbative quantum chromodynamics (PQCD) corrections in the calculations. Several Monte Carlo event generators based on the k_T-factorization formalism, like CASCADE [7], KATIE [8], and PEGASUS [9], are developed and a number of corresponding phenomenological applications are known in the literature. Thus, the k_T-factorization approach becomes an essential tool which allows one to make theoretical predictions for future experiments at modern (LHC) and future (FCC, EiC, EicC) colliders.

In this sense, special interest is connected with the selection of the TMD parton density in the proton best

Published by the American Physical Society under the terms of the Creative Commons Attribution 4.0 International license. Further distribution of this work must maintain attribution to the author(s) and the published article's title, journal citation, and DOI. Funded by SCOAP³.

suited to describe the currently available collider data and which therefore can be used to generate the necessary realistic predictions. However, in contrast to much of our knowledge about the conventional PDFs accumulated in theoretical and experimental studies over the past years, the TMD parton densities are still poorly known quantities. There are some popular approaches to evaluate the latter, for example, the Kimber-Martin-Ryskin prescription [10,11], Balitsky-Kovchegov [12] or Gribov-Levin-Ryskin (GLR) [13] evolution equations,[1] CCFM-based formalism [15], and the parton branching (PB) approach [16,17]. A variety of currently available TMD sets are collected in the TMDLIB package [18], which is a C++ library providing a framework and an interface for the different parametrizations.

It is known that the appropriate choice of the nonperturbative input $f_a^{(0)}(x,\mathbf{k}_T^2,\mu_0^2)$, which is used as the initial condition for subsequent QCD evolution [19–22], plays an important role in the derivation of TMD parton densities in a proton. In fact, its influence on the description of experimental data can be significant [23–26]. Similar to collinear PDFs, starting TMD parton distributions are usually parametrized in a rather general form (see Sec. II below) and then fitted to some experimental data. Such procedures were carried out for the CCFM [15] and PB [27] approaches with the XFITTER tool [28], where the latest precision HERA measurements of the proton structure function $F_2(x,Q^2)$ were used. In contrast, in our previous studies [23–26], the modified soft quark-gluon string model (QGSM) [29,30] was applied to determine the parameters of an analytical expression for the starting TMD gluon density in a proton $f_g^{(0)}(x,\mathbf{k}_T^2,\mu_0^2)$. In the modified QGSM, both the longitudinal and transverse motion of quarks and gluons [31,32] as well as the saturation effects at small x and low scales can be taken into account. The essential phenomenological parameters were obtained from the best description of RHIC and LHC data on the inclusive spectra of hadrons produced in pp and AA collisions at low transverse momenta, and the CCFM evolution equation was applied to extend the proposed TMD gluon density in the whole kinematical region. It was shown that such an approach is able to describe the HERA data on proton structure functions $F_2^c(x,Q^2)$, $F_2^b(x,Q^2)$, and $F_L(x,Q^2)$ and LHC data on several processes, in particular, single top production and inclusive Higgs boson production at $\sqrt{s}=8$ and 13 TeV.

In the present paper, we continue our study and recalculate $f_g^{(0)}(x,\mathbf{k}_T^2,\mu_0^2)$ more accurately using the modified QGSM. Moreover, we determine the parameters of the initial gluon density using the LHC data on soft hadron (kaon and pion), inclusive b-jet and Higgs boson production in pp collisions at different energies as well as the latest HERA data on proton structure functions $F_2^c(x,Q^2)$ and $F_2^b(x,Q^2)$ and reduced cross sections $\sigma_{\rm red}^c(x,Q^2)$ and $\sigma_{\rm red}^b(x,Q^2)$. Thus, we take a step toward the global fit of the TMD gluon density from the collider data that significantly improves our earlier analyses [23–26].

The paper is organized as follows. In Sec. II, we briefly describe our theoretical input and discuss the basic steps of the calculations of soft hadron spectra in the modified QGSM. Then, from the best description of the LHC data on the latter, we derive an updated analytical expression for the initial TMD gluon density in a proton. In Sec. III, we perform a fit of several phenomenological parameters from the LHC and HERA data and compare our results with the known ones. We give conclusions in Sec. IV.

II. THE MODEL

Similar to conventional PDFs, a construction of the TMD parton distributions in a proton starts from the input densities, which are further used as the initial conditions for subsequent noncollinear QCD evolution. As mentioned above, usually the initial TMD gluon density at some starting scale μ_0^2 (which is of order of the hadron scale) is taken in the rather general empirical form with factorized Gauss smearing in transverse momentum $\mathbf{k}_T^2$ (see, for example, [15]):

$$f_g^{(0)}(x,\mathbf{k}_T^2,\mu_0^2)=a_1x^{a_2}(1-x)^{a_3}e^{-\mathbf{k}_T^2/q_0^2}, \tag{1}$$

where all the parameters have to be extracted from the experimental data. Alternatively, a more physically motivated nonfactorized expression for $f_g^{(0)}(x,\mathbf{k}_T^2,\mu_0^2)$ can be taken from the Golec-Biernat-Wüsthoff (GBW) approach [33,34] based on color dipole picture for DIS:

$$f_g^{(0)}(x,\mathbf{k}_T^2,\mu_0^2)=c_gR_0^2(x)\mathbf{k}_T^2e^{-R_0^2(x)\mathbf{k}_T^2},$$
$$R_0(x)=\frac{1}{Q_0}\left(\frac{x}{x_0}\right)^{\lambda/2}, \tag{2}$$

where $c_g=3\sigma_0/(4\pi^2\alpha_s)$, $\sigma_0=29.12$ mb, $\alpha_s=0.2$, $Q_0=1$ GeV, $x_0=4.1\times10^{-5}$, and $\lambda=0.277$. In this approach, the effect of the saturation of the $q\bar{q}$ dipole cross section at large distance r between the quark and antiquark in the dipole or small μ is assumed. This saturation of the dipole cross section is a direct consequence of the saturation of the cross section of virtual photon-proton scattering (γ^*p) [33]. It leads to the scale-independent behavior of the TMD gluon density $f_g^{(0)}(x,\mathbf{k}_T^2,\mu_0^2)$ at $\mu<\mu_{\rm sat}$, where $\mu_{\rm sat}$ is the saturation scale. The GBW model was successfully applied to both inclusive and diffractive ep scattering at HERA. However, we face some difficulties in determining an accurate description of several hard LHC processes.

[1]Very recently, a new Monte Carlo algorithm to simulate the initial state parton branching in the small-x region according to the GLR equation has been proposed [14].

In our previous studies [23–25], to describe successfully the LHC data on soft hadron production in pp collisions, we modified the starting form of the gluon density (2) as the following:

$$f_g^{(0)}(x,\mathbf{k}_T^2,\mu_0^2) = c_0 c_1 (1-x)^b [R_0^2(x)\mathbf{k}_T^2 + c_2 (R_0^2(x)\mathbf{k}_T^2)^{a/2}] \times \exp\left(-R_0(x)|\mathbf{k}_T| - d[R_0^2(x)\mathbf{k}_T^2]^{3/2}\right). \quad (3)$$

Then, to extend the consideration to a region of larger p_T we added to (3) some function dependent on k_T and low x, which was matched with the exact solution [35] of the BFKL equation outside of the saturation region. As we mentioned above, in this way one could provide a reasonably good description [26] of some HERA and LHC data using the proposed analytical expression (nonfactorized with respect to x and $\mathbf{k}_T^2$) for the initial TMD gluon density with parameters obtained in the modified QGSM approach [31,32]. However, in the present paper we suggest a new approach for the calculation of p_T spectra of soft hadron production. Below, we discuss our suggestion based on the scale-independent behavior of the starting gluon density $f_g^{(0)}(x,\mathbf{k}_T^2,\mu_0^2)$ at $\mu \le \mu_0$ and low x. After that, we find the corresponding phenomenological parameters from the best description of soft hadron spectra measured at different LHC energies. For the reader's convenience, below we briefly recall the basic formulas with a short review of the calculation steps.

A. Hadron spectra at low p_T in the midrapidity region

As is well known, the soft hadron production in pp collisions at small momentum transfer and large Feynman variables x_F can be analyzed successfully within the soft QCD models, such as the QGSM [29,30] or dual parton model [36]. It is based on the Regge behavior of the cross section at large x_F. In the QGSM, the interaction dynamics is based on two colorless strings formed between the quark/diquark (q/qq) and diquark/quark (qq/q) of the colliding protons.[2] At their breaking, the quark-antiquark and diquark-antidiquark pairs are created in the chromostatic QCD field, and then they fragment into final hadrons h. The corresponding quark and diquark distribution functions and their fragmentation functions into hadrons were calculated [29,30]. Such an approach allows one to describe the experimental observables at nonzero x_F and low transverse momenta p_T quite satisfactorily.

In the midrapidity region, according to the Abramovsky-Gribov-Kancheli (AGK) cutting rules [37], only one-Pomeron Mueller-Kancheli diagrams contribute to the inclusive hadron spectrum. However, we face some difficulties in determining a description of inclusive hadron spectra measured in this kinematical region. In fact, the predicted hadron transverse momentum distributions fall down very fast with the increase of p_T compared to the data [32]. To avoid these difficulties, the QGSM was modified [31,32]. So, it was suggested that there are soft gluons in a proton which split into $q\bar{q}$ pairs and therefore give additional contribution to the hadron spectrum. The contribution of the one-Pomeron exchange graph between gluons in the colliding protons and the contribution of one-Pomeron Mueller-Kancheli diagrams to the inclusive p_T spectrum were taken into account. However, the application of the AGK cutting rules in the case where soft gluons as well as quarks are included in the calculation is very questionable. In [31,32], these contributions of quarks, diquarks, and gluons were calculated separately, independent of each other assuming that the contribution of gluons to the spectrum vanishes at zero transverse momenta of the produced hadrons. Additionally, the splitting function of gluons into $q\bar{q}$ pairs was calculated ignoring the dependence of gluon distribution on the transverse momentum k_T. Therefore, in this paper we recalculate the inclusive p_T spectra of charged hadrons produced in pp collisions at midrapidity and small p_T.

As mentioned above, the data [38,39] on the $\gamma^* p$ cross section show its saturation at low Q^2 and low x [33]. It leads to the saturation of the dipole cross section and scale-independent behavior of the starting gluon density at low Q^2 less than the saturation transfer square $Q^2_{\rm sat}$. Therefore, the colliding protons at low Q^2 can be considered as two systems consisting of three valence quarks and a gluon environment with the wave function Ψ_g, and its square is related to the starting gluon distribution as $|\Psi_g|^2 \sim \tilde{f}_g^{(0)}(x,\mathbf{k}_T^2,\mu_0^2)$. Then, the pp interaction amplitude can be presented in the simple spectator form $F_{pp} = f_{3q}^{(0)}\Psi_g$, where $f_{3q}^{(0)}$ is the amplitude of the interaction of two $3q$ systems. To calculate the inclusive spectrum $\rho(x,p_T) \equiv E\frac{d^3\sigma}{d^3\mathbf{p}} \equiv \frac{1}{\pi}\frac{d^3\sigma}{d^2p_T dy}$ of hadrons h, we have to calculate the sum of the quark contribution ρ_q and the gluon one ρ_g, i.e.,

$$\rho(x,p_T) = \rho_q(x,p_T) + \rho_g(x,p_T). \quad (4)$$

The first term in (4) was calculated within the QGSM [29,30] using only the one-Pomeron exchange or the cylinder graph because in the midrapidity and small $x_T = 2p_T/\sqrt{s}$ the multi-Pomeron exchanges result in negligibly small contributions, as shown in [32]. It is presented in the following form:

$$\rho_q(s,x,p_T) = \sigma_1 \phi_q(s,x,p_T), \quad (5)$$

where σ_1 is the cross section of the one-Pomeron exchange (see [29] and references therein)

[2]These two colorless strings can be stretched between valence quarks and diquarks corresponding to the one-Pomeron exchange between colliding protons. Also, many strings can be stretched between sea quarks and antiquarks in the interacting protons, which correspond to n-Pomeron exchanges.

$$\sigma_1 = \frac{\sigma_P}{z}(1-e^{-z}), \qquad \sigma_P = 8\pi\gamma_P(s/s_0)^{\Delta},$$
$$z = \frac{2C\gamma_P(s/s_0)^{\Delta}}{R^2+\alpha'_P \ln s/s_0}. \tag{6}$$

All the parameters in (6) are found [40] from experimental data on the total and differential cross sections of elastic pp and $p\bar{p}$ scattering at high energies: $\gamma_P = 1.27$ GeV^{-2}, $\Delta = 0.156$, $C = 1.8$, $R^2 = 4.0$ GeV^{-2}, $\alpha'_P = 0.25$ GeV^{-2}. The function $\phi_q(s,x,p_T)$ is calculated within the QGSM and presented in Eq. (8). The second one, $\rho_g(x,p_T)$, is the convolution of the modified gluon distribution $F_g(x,k_T)$ with the fragmentation function of gluons to hadrons $D_{g\to h}$ multiplied by the integral from $|f_{3q}^{(0)}|^2$ over the intrinsic phase space, which results in approximately the inelastic pp cross section $\sigma_{\rm in}^{pp}$ because the LHC data described in this paper exclude the elastic pp collisions. The modified gluon distribution $F_g(x,k_T)$ as well as the modified quark and diquark distributions $F_q(x,k_T), F_{qq}(x,k_T)$ are calculated taking into account the energy-momentum conservation law; see Eqs. (15)–(20). So, we can write

$$\rho_g(x,p_T) = F_g \otimes D_{g\to h} \times \sigma_{\rm in}^{pp}. \tag{7}$$

Finally the hadron spectrum at low x and low p_T can be presented as the following:

$$\rho(x,p_T) = \sigma_1\phi_q(s,x,p_T) + \sigma_{\rm in}\phi_g(s,x,p_T). \tag{8}$$

The first and second terms in (8) represent the quark/diquark and gluon contributions, respectively,

$$\phi_q(s,x,p_T) = \{\Phi_q(x_+,p_T)\Phi_{qq}(x_-,p_T) + \Phi_{qq}(x_+,p_T)\Phi_q(x_-,p_T)\}, \tag{9}$$

$$\phi_g(s,x,p_T) = \{\Phi_g(x_+,p_T) + \Phi_g(x_-,p_T)\}, \tag{10}$$

where

$$x_\pm = \frac{1}{2}(\pm x + \sqrt{x^2 + 4(m_h^2+p_T^2)/s}),$$
$$x = 2\sqrt{\frac{m_h^2+p_T^2}{s}}\sinh y, \tag{11}$$

m_h is the produced hadron mass, and the phenomenological parameters C_q and C_g have to be determined from the data. Keeping in mind that the proton consists of two up quarks and one down quark and taking into account the nonzero parton transverse momenta, the contributions of the quark, diquark, and gluon fragmentations within the modified QGSM approach are calculated as convolutions [31,32]:

$$\Phi_q(x,p_T) = \int_x^1 d\xi \int_0^\infty d\mathbf{k}_T^2 \int_0^{2\pi} d\phi \times \left[\frac{2}{3}F_u(\xi,\mathbf{k}_T^2)G_{u\to h}(z,|\mathbf{p}_T - z\mathbf{k}_T|) + \frac{1}{3}F_d(\xi,\mathbf{k}_T^2)G_{d\to h}(z,|\mathbf{p}_T - z\mathbf{k}_T|)\right], \tag{12}$$

$$\Phi_{qq}(x,p_T) = \int_x^1 d\xi \int_0^\infty d\mathbf{k}_T^2 \int_0^{2\pi} d\phi \times \left[\frac{2}{3}F_{ud}(\xi,\mathbf{k}_T^2)G_{ud\to h}(z,|\mathbf{p}_T - z\mathbf{k}_T|) + \frac{1}{3}F_{uu}(\xi,\mathbf{k}_T^2)G_{uu\to h}(z,|\mathbf{p}_T - z\mathbf{k}_T|)\right], \tag{13}$$

$$\Phi_g(x,p_T) = \int_x^1 d\xi \int_0^\infty d\mathbf{k}_T^2 \int_0^{2\pi} d\phi F_g(\xi,\mathbf{k}_T^2) \times G_{g\to h}(z,|\mathbf{p}_T - z\mathbf{k}_T|), \tag{14}$$

where $\mathbf{k}_T$ is the transverse momentum of the quark, diquark, and/or gluon, $z = x/\xi$, and ϕ is the azimuthal angle between $\mathbf{p}_T$ and $\mathbf{k}_T$. The quark, diquark, and gluon fragmentation functions to hadrons (namely, to pions and kaons), $G_{a\to h}(z,|\mathbf{p}_T|)$ with $a = q$, qq, or g, were calculated in the QGSM at leading- (LO) and next-to-leading (NLO) orders [41]. The corresponding analytical expressions are collected in Appendix A. The functions $F_a(x,\mathbf{k}_T^2)$ involved in (12)–(14) are related to the TMD parton distributions in a proton taken at some scale determined by the produced hadron transverse momentum.[3] The functions $F_q(x,\mathbf{k}_T^2)$, $F_{qq}(x,\mathbf{k}_T^2)$, and $F_g(x,\mathbf{k}_T^2)$ were calculated using the energy-momentum conservation law for the quark, diquark, and gluon. So, for example,

$$F_q(x,\mathbf{k}_T^2) = \int_{x_\pm}^1 d\xi_1 d\xi_2 \delta(1-x-\xi_1-\xi_2) \times \int d^2\mathbf{p}_T d^2\mathbf{q}_T \delta^{(2)}(\mathbf{k}_T + \mathbf{p}_T + \mathbf{q}_T) \times \tilde{f}_q(x,\mathbf{k}_T^2)\tilde{f}_{qq}(\xi_1,\mathbf{p}_T^2)\tilde{f}_g(\xi_2,\mathbf{q}_T^2), \tag{15}$$

where $\tilde{f}_a(x,\mathbf{k}_T^2) \equiv f_a(x)g_a(\mathbf{k}_T^2)$ and $\tilde{f}_g(x,\mathbf{k}_T^2) \equiv f_g(x,\mathbf{k}_T^2)/x$ are the k_T-dependent quark, diquark, and gluon densities, respectively (see below). Performing integration over ξ_1 and $\mathbf{p}_T^2$ in (15), one can easily obtain

[3] As mentioned above, this scale could be considered as the starting scale for subsequent QCD evolution due to small hadron transverse momentum, $p_T \sim 1$ GeV.

$$F_u(x,\mathbf{k}_T^2) = \tilde{f}_u(x) g_q(\mathbf{k}_T^2) \int_{x_\pm}^{1-x} d\xi_2 \int_0^\infty d\mathbf{q}_T^2 \int_0^{2\pi} d\varphi \times \tilde{f}_{ud}(1-x-\xi_2) g_{qq}(|\mathbf{k}_T+\mathbf{q}_T|^2) \tilde{f}_g(\xi_2,\mathbf{q}_T^2), \tag{16}$$

$$F_d(x,\mathbf{k}_T^2) = \tilde{f}_d(x) g_q(\mathbf{k}_T^2) \int_{1x_\pm}^{1-x} d\xi_2 \int_0^\infty d\mathbf{q}_T^2 \int_0^{2\pi} d\varphi \times \tilde{f}_{uu}(1-x-\xi_2) g_{qq}(|\mathbf{k}_T+\mathbf{q}_T|^2) \tilde{f}_g(\xi_2,\mathbf{q}_T^2), \tag{17}$$

where φ is the azimuthal angle between $\mathbf{k}_T$ and $\mathbf{q}_T$. Similarly, one can derive expressions for $F_{qq}(x,\mathbf{k}_T^2)$:

$$F_{ud}(x,\mathbf{k}_T^2) = \tilde{f}_{ud}(x) g_{qq}(\mathbf{k}_T^2) \int_{x_\pm}^{1-x} d\xi_2 \int_0^\infty d\mathbf{q}_T^2 \int_0^{2\pi} d\varphi \times \tilde{f}_u(1-x-\xi_2) g_{qq}(|\mathbf{k}_T+\mathbf{q}_T|^2) \tilde{f}_g(\xi_2,\mathbf{q}_T^2), \tag{18}$$

$$F_{uu}(x,\mathbf{k}_T^2) = \tilde{f}_{uu}(x) g_{qq}(\mathbf{k}_T^2) \int_{x_\pm}^{1-x} d\xi_2 \int_0^\infty d\mathbf{q}_T^2 \int_0^{2\pi} d\varphi \times \tilde{f}_d(1-x-\xi_2) g_{qq}(|\mathbf{k}_T+\mathbf{q}_T|^2) \tilde{f}_g(\xi_2,\mathbf{q}_T^2). \tag{19}$$

For $F_g(x,\mathbf{k}_T^2)$, we have the following formula including the charge and isotopic invariance:

$$F_g(x,\mathbf{k}_T^2) = \tilde{f}_g(x,\mathbf{k}_T^2) \int_{x_\pm}^{1-x} d\xi_2 \int_0^\infty d\mathbf{q}_T^2 \int_0^{2\pi} d\varphi \left\{ \frac{2}{3} \tilde{f}_u(1-x-\xi_2) g_q(|\mathbf{k}_T+\mathbf{q}_T|^2) \tilde{f}_{ud}(\xi_2) g_{qq}(\mathbf{q}_T^2) + \frac{1}{3} \tilde{f}_d(1-x-\xi_2) g_q(|\mathbf{k}_T+\mathbf{q}_T|^2) \tilde{f}_{uu}(\xi_2) g_{qq}(\mathbf{q}_T^2) \right\}. \tag{20}$$

The distributions f_u, f_d, f_{uu}, f_{ud}, and g_q, g_{qq} as functions of x and k_T, respectively, are presented in Appendix A. Our choice for the TMD parton densities involved in (16)–(20) is particularly discussed in Sec. II. 2.

Finally, the inelastic pp cross section $\sigma_{\rm in}$ can be calculated as the difference between the total and elastic pp scattering cross sections: $\sigma_{\rm in} = \sigma_{\rm tot} - \sigma_{\rm el}$, where $\sigma_{\rm tot}$ should satisfy the Regge asymptotic $\sigma_{\rm tot} \sim (s/s_0)^{\alpha_P - 1}$. However, it was shown [42,43] that $\sigma_{\rm tot}$ and $\sigma_{\rm el}$ can be parametrized in the following way:

$$\sigma_{\rm tot} = 21.7(s/s_0)^{0.0808} + 56.08(s/s_0)^{-0.4525} \text{ mb}, \tag{21}$$

$$\sigma_{\rm el} = 11.84 - 1.617 \ln s + 0.1359 \ln^2 s \text{ mb}, \tag{22}$$

where $s_0 = 1$ GeV. Therefore, we will use these expressions in the numerical calculations.

Using the expressions above, one can calculate the cross sections for soft hadron production in pp collisions. Some technical details are given in Appendix B. To perform numerical multidimensional integration, we employ a Monte Carlo technique implemented with the VEGAS tool [44].

B. TMD parton distributions in a proton at low scale

Concerning the TMD gluon density $f_g(x,\mathbf{k}_T^2)$, here we will follow our previous considerations [23–26] where the different expressions based on the GBW saturation model were tried. In fact, it was demonstrated that the overall description of collider data could be significantly improved if the usual GBW gluon distribution given by (2) is modified. In the present analysis, we update the modification proposed earlier [23,24] and take into account a certain quark-gluon sum rule[4]:

$$\sum_a \int_0^1 dx \int d^2\mathbf{k}_T x \tilde{f}_a(x,\mathbf{k}_T^2) = 1, \tag{23}$$

where $a = u$, d, uu, ud, and g.

We will consider the data on charged hadron (pion and kaon) production at small transverse momenta $p_T \leq 1$ GeV taken at different energies, namely, $\sqrt{s} = 0.9$, 2.36, 7, and 13 TeV [45–47]. We find that in order to describe these data, the most appropriate expression for the starting gluon density $f_g(x,\mathbf{k}_T^2.\mu_0^2)$, hereafter labeled as the LLM gluon, is the following:

$$f_g(x,\mathbf{k}_T^2) = c_g(1-x)^{b_g} \sum_{n=1}^{3} (c_n R_0(x)|\mathbf{k}_T|)^n e^{-R_0(x)|\mathbf{k}_T|}, \tag{24}$$

where $R_0(x)$ is defined in (2), and we kept $x_0 = 4.1 \times 10^{-5}$ and $\lambda = 0.22$. Our best fit for phenomenological parameters leads to $c_1 = 5$, $c_2 = 3$, $c_3 = 2$, and $Q_0 = 1.233$ GeV. We have specially checked that some variation in x_0 and λ does not affect the fit quality. However, the measured

[4]The TMD gluon density used in [25,26] has a very high $\mathbf{k}_T^2$ tail, that leads to sizeable value of gluon average transverse momentum. The latter, of course, should have a significant perturbative component unwanted for our purposes.

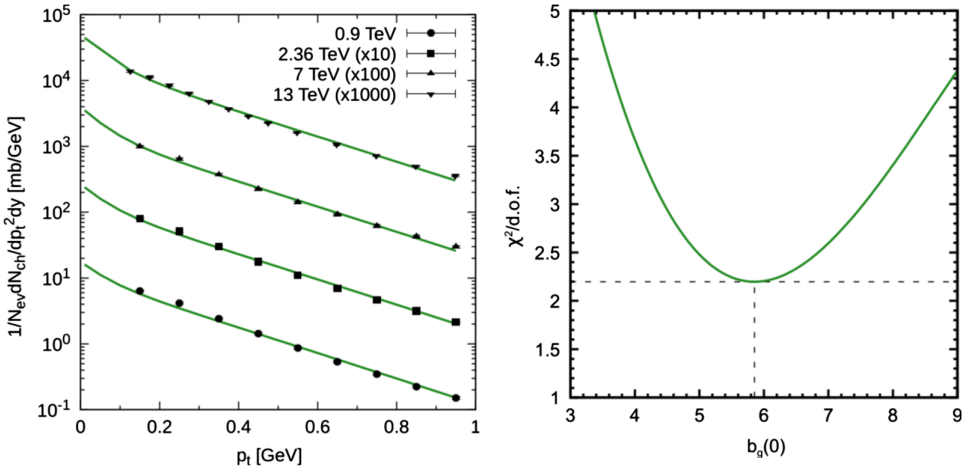

FIG. 1. Left panel: charged hadron spectra calculated within the modified QGSM at different energies. Experimental data are from [45–47]. Right panel: χ^2/d.o.f. dependence of our fit performed moderate- and large-x values.

hadron spectra [45–47] refer to a relatively small-x region and appear to be mostly insensitive to the b_g value, which plays a role at essentially larger x. So, we determined the latter from the LHC data on several hard processes, as described in Sec. III. Following [48,49], we treat b_g as a running parameter at $\mathbf{k}_T^2 \geq Q_0^2$:

$$b_g = b_g(0) + \frac{4C_A}{\beta_0} \ln \frac{\alpha_s(Q_0^2)}{\alpha_s(\mathbf{k}_T^2)}, \tag{25}$$

where $b_g(0) = 5.854$, $C_A = N_c$, and $\beta_0 = 11 - 2/3N_f$ is the first coefficient of the QCD β function. At small $\mathbf{k}_T^2 < Q_0^2$, the fixed value $b_g = b_g(0)$ is used. A similar approach was applied in the investigation of the European Muon Collaboration effect from the study of shadowing at low x to antishadowing at $x \sim 0.1$–0.2 [50].

The experimental data on the charged hadron production involved in the fit are compared with our predictions in Fig. 1 (left panel). One can see that good agreement is achieved in a wide range of energies.

C. Saturation dynamics

As it is assumed in [33,34], the effective dipole cross section as a function of the distance r between q and $\bar{q}$ is saturated at large r. It is presented in the following form:

$$\hat{\sigma}(x, r^2) = \sigma_0 \left\{ 1 - \exp\left(-\frac{r^2}{4R_0^2(x)} \right) \right\}, \tag{26}$$

where R_0 is determined in (2). The normalization σ_0 and the parameters λ and x_0 were found from a fit of all inclusive DIS data [33,34]. The relation of the TMD gluon distribution to the dipole cross section $\hat{\sigma}(x, r^2)$ was calculated [34] within the two-gluon exchange approximation between $q, \bar{q}$ and the nucleon debris. It has the following form:

$$\hat{\sigma}(x, r^2) = \frac{4\pi^2}{3} \int \frac{dk_t^2}{k_t^2} \{1 - J_0(k_T r)\} \alpha_s(\mu_0^2) f_g^{(0)}(x, \mathbf{k}_T^2, \mu_0^2), \tag{27}$$

where $J_0(k_T r)$ is the cylindrical special function of order 0. Comparing (26) to (27), one can immediately get the expression (2).

Inserting our gluon distribution (LLM) at the initial μ_0 presented in (24)–(27), one can get the dipole cross section at different values of x as a function of r, which is proportional to $2/Q_0$ according to [34]. In Fig. 2 (left panel), the comparison of the GBW dipole cross section $\hat{\sigma}(x, r^2)$ calculated using (2) to our calculation (24) is presented as a function of r at different x. One can see that the saturation of the dipole cross section at large r strongly depends on x and on the TMD gluon density. The GBW gluon density results in the saturation scale $r_s \sim 2/R_0$ according to (26) [34]. According to Fig. 2, the saturation scale corresponding to the GBW gluon density at $x = 4.2 \times 10^{-5}$ is $Q_s \simeq 2/r_s \simeq 0.8$ GeV, whereas the LLM gluon density results in $Q_s \simeq 2/r_s \simeq 0.4$ GeV at the same x. It means that at $Q^2 < Q_s^2$, the dipole cross section and starting gluon density do not depend on scale Q^2.

Let us note that the GBW and LLM gluon densities vanish at $k_T \to 0$. It is due to the neglecting of the initial gluon mass m_g in the gluon propagator; see (27) and [34]. With the inclusion of the gluon mass, the TMD gluon distributions does not vanish at zero gluon transverse momentum. However, $f_g^{(0)}(x, \mathbf{k}_T^2, \mu_0^2)$ does not vanish at $k_T = 0$ even at $m_g = 100$ MeV according to Fig. 2 (right panel).

D. CCFM evolution

Being sure that proposed TMD gluon density in a proton is able to reproduce well the collider data in a soft

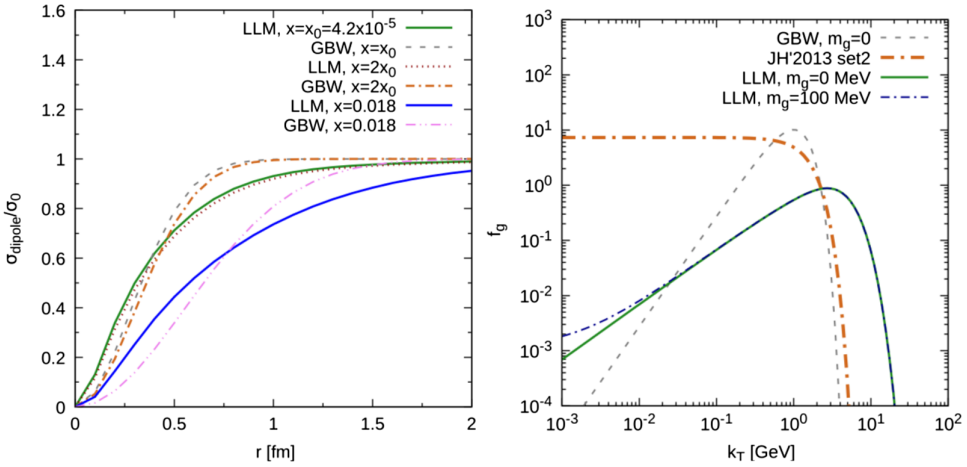

FIG. 2. Left: the dipole cross section as a function of r at different values of x. Right: the LLM and GBW gluon densities as functions of k_T at different gluon masses. The JH'2013 set 2 [15] gluon distribution is presented for comparison.

kinematical region, one can consider the expression (24) as the starting condition for subsequent QCD evolution.

As mentioned above, we will apply the CCFM equation [4]. It resums both large logarithms $\alpha_s^n \ln^n 1/x$ and $\alpha_s^n \ln^n 1/(1-x)$ and introduces an angular ordering condition to treat the gluon coherence effects correctly. In the limit of asymptotic high energies (i.e., small x), it is almost equivalent to BFKL [3], but it is also similar to the usual DGLAP evolution [1] for large x, smoothly interpolating between these two kinematical regimes. Therefore, it provides a suitable tool for our purposes.[5]

In the leading logarithmic approximation, the CCFM equation for TMD gluon density[6] $f_g(x, \mathbf{k}_T^2, \mu^2)$ can be written as

$$f_g(x,\mathbf{k}_T^2,\mu^2) = f_g^{(0)}(x,\mathbf{k}_T^2,\mu_0^2)\Delta_s(\mu,\mu_0) + \int \frac{dz}{z}\int \frac{dq^2}{q^2}\Theta(\mu - zq)\Delta_s(\mu,zq) \times \tilde{P}_{gg}(z,\mathbf{k}_T^2,q^2) f_g\left(\frac{x}{z},\mathbf{k}_T'^2,q^2\right), \quad (28)$$

where $\mathbf{k}_T' = \mathbf{q}(1-z) + \mathbf{k}_T$ and $\tilde{P}_{gg}(z,\mathbf{k}_T^2,q^2)$ is the CCFM splitting function:

$$\tilde{P}_{gg}(z,\mathbf{k}_T^2,q^2) = \bar{\alpha}_s(q^2(1-z)^2)\left[\frac{1}{1-z} + \frac{z(1-z)}{2}\right] + \bar{\alpha}_s(\mathbf{k}_T^2)\left[\frac{1}{z} - 1 + \frac{z(1-z)}{2}\right]\Delta_{ns}(z,\mathbf{k}_T^2,q^2). \quad (29)$$

The Sudakov and non-Sudakov (or Regge) form factors read

$$\ln\Delta_s(\mu,\mu_0) = -\int_{\mu_0^2}^{\mu^2}\frac{d\mu'^2}{\mu'^2}\int_0^{1-\mu_0/\mu'} d\zeta \frac{\bar{\alpha}_s(\mu'^2(1-\zeta)^2)}{1-\zeta}, \quad (30)$$

$$\ln\Delta_{ns}(z,\mathbf{k}_T^2,\mathbf{q}_T^2) = -\bar{\alpha}_s(\mathbf{k}_T^2)\int_0^1 \frac{dz'}{z'}\int\frac{dq^2}{q^2} \times \Theta(\mathbf{k}_T^2 - q^2)\Theta(q^2 - z'^2\mathbf{q}_T^2), \quad (31)$$

where $\bar{\alpha}_s = 3\alpha_s/\pi$. The first term in (28) is the initial TMD gluon density $f_g^{(0)}(x,\mathbf{k}_T^2,\mu_0^2)$ determined at the scale μ_0^2 multiplied by the Sudakov form factor describing the contribution of nonresolvable branchings between the starting scale μ_0^2 and scale μ^2. In our calculations, the expression (24) will be used as the initial gluon density. The second term represents the details of the QCD evolution expressed by the convolution of the CCFM gluon splitting function $\tilde{P}_{gg}(z,\mathbf{k}_T^2,q^2)$ with the TMD gluon density and Sudakov form factor. The angular ordering condition is introduced with the theta function, so the evolution scale μ^2 is coming from the maximum allowed angle for any gluon emission determined by the hard scattering subprocess $\mu^2 = \hat{s} + \mathbf{Q}_T^2$, where $\mathbf{Q}_T$ is the net transverse momentum entering the hard subprocess with center-of-mass energy $\hat{s}$. This choice for scale μ^2 is usually considered as a built-in property of the CCFM evolution (see, for example, [15] and references therein).

The CCFM equation can be solved numerically using the UPDFEVOLV routine [51], so that the TMD gluon density can be obtained in the whole kinematical range. In this way, the TMD gluon distribution is tabulated in a commonly recognized format (namely, a grid of $50\times50\times50$ bins in x, $\mathbf{k}_T^2$, and μ^2) which is used in the TMDLIB tool [18].

[5]We note that the proposed approach can be used, in principle, with other QCD evolution scenarios employing TMD parton dynamics in a proton, such as the PB [27] or GLR [13] framework.

[6]Hereafter, we denote the evolution variable as μ^2. Another notation, namely, $\bar{q}^2$, is also often used in the literature.

III. FITTING THE ESSENTIAL PARAMETERS

There are phenomenological parameters in the initial TMD gluon density (24) which are not predicted by the theory and therefore have to be extracted from the collider data. Our fitting strategy is based on splitting the overall procedure into two almost independent parts, where each of them refers to the regions of low and large x, respectively. This is because the measured normalized hadron spectra considered in Sec. II. 2 are almost insensitive to the overall normalization given by c_g and to the shape parameter $b_g(0)$, which plays a role mainly at moderate and large x values. So, now we turn to this region and refine the behavior of the proposed gluon distribution by extracting the c_g and $b_g(0)$ parameters from the measured cross sections of some hard processes. We will use the CMS data on inclusive b-jet production in pp collisions at $\sqrt{s} = 7$ TeV [52] and recent data on inclusive Higgs boson production in different decay modes taken by the ATLAS [53,54] and CMS [55] Collaborations at $\sqrt{s} = 13$ TeV. The cross sections of these processes are governed by gluon-gluon fusion subprocesses and receive an essential contribution, in particular, from the appropriate x region.[7] In fact, the CMS data on b-jet production refer to the kinematical region defined by $18 < p_T(b) < 196$ GeV and rapidity $|y(b)| < 2.2$ [52]. The ATLAS data on inclusive Higgs production in the diphoton decay mode were obtained at $p_T^\gamma/m^{\gamma\gamma} > 0.35$ (0.25) for the leading (subleading) decay photon, pseudorapidity $|\eta^\gamma| < 2.37$ for both photons, and the invariant mass $105 < m^{\gamma\gamma} < 160$ GeV [53]. The CMS data refer to a similar kinematical region: $p_T^\gamma/m^{\gamma\gamma} > 1/3$ (1/4) for the leading and subleading photons $|\eta^\gamma| < 2.5$ and $100 < m^{\gamma\gamma} < 180$ GeV [55]. The ATLAS measurement [54] performed in the $H \to ZZ^* \to 4l$ decay mode requires at least four leptons in the event with at least one lepton having $p_T > 20$ GeV, another lepton having $p_T > 15$ GeV, and the remaining ones having $p_T > 10$ and 5 GeV, respectively. All leptons must have the pseudorapidity $|\eta(l)| < 2.7$, the leading pair invariant mass m_{12} must be $50 < m_{12} < 106$ GeV, and the subleading one should be $12 < m_{34} < 115$ GeV. Finally, the four-lepton invariant mass m_{4l} must satisfy the $105 < m_{4l} < 160$ GeV cut. Thus, the typical x values probed in these analyses $x \sim 2\mu/\sqrt{s}$ are varied from $x \sim 5 \times 10^{-3}$ to $x \sim 2 \times 10^{-2}$, where the scale μ of the considered processes is determined, for example, by the transverse masses of the produced particles. Additionally, we use the latest HERA data on the charm and beauty contributions to the inclusive proton structure functions $F_2^c(x, Q^2)$, $F_2^b(x, Q^2)$ [57–59], and reduced cross sections $\sigma_{\rm red}^c(x, Q^2)$ and $\sigma_{\rm red}^b(x, Q^2)$ [60] obtained at $Q^2 > 2.5$ GeV^2 in a wide region of x. The DIS reduced cross section of the heavy quark Q can be presented as

$$\sigma_{\rm red}^Q(x, Q^2) = F_2^Q(x, Q^2) - \frac{y^2}{1 + (1-y)^2} F_L^Q(x, Q^2), \quad (32)$$

where $y = Q^2/(xS)$, and $F_L^Q(x, Q^2)$ is the contribution of the heavy quark Q to the proton longitudinal structure function $F_L(x, Q^2)$. All of these observables are governed by photon-gluon fusion subprocess, and therefore, they are also very sensitive to the gluon content of a proton. Note that, in contrast with another study [15], we do not consider the latest precise HERA data on the inclusive proton structure function $F_2(x, Q^2)$, since the latter could include a sizeable quark component.

We extracted the c_g and $b_g(0)$ values from the best simultaneous description of several observables, in particular, the distributions on leading b-jet transverse momenta measured at their different rapidities, Higgs boson transverse momentum, and rapidity spectra. We also considered several angular correlations in Higgs boson production, namely, distributions on the Higgs decay photon helicity angle (in the Collins-Soper frame), leading lepton pair decay angle with respect to the beam axis (in the four-lepton rest frame), and production angles of antileptons from the two-decay Z bosons, where these angles are defined relative to the Z direction. The fitting procedure is rather standard and straightforward. Technically, applying the UPDEVOLV routine [51], we solved numerically the CCFM equation for a (large) number of fixed guessed $b_g(0)$ values in a wide (but still reasonable) range $3 < b_g(0) < 8$. Then, using each of the generated TMD gluon densities in the proton, we calculated the cross sections of all considered processes according to previous evaluations [61–63]. The best simultaneous description of the experimental data for all observables above is achieved at $c_g = 0.173 \pm 0.009$ and $b_g(0) = 5.854^{+1.920}_{-1.553}$ with $\chi^2/\text{d.o.f.} = 2.2$; see Fig. 1. Note that we took into account the contributions to the Higgs production cross sections from weak boson fusion ($W^+W^- \to H$ and $ZZ \to H$) associated HZ or $HW^\pm$ production and associated $t\bar{t}H$ production. These contributions are essential at high transverse momenta and have been calculated in the conventional NLO PQCD. We took them from [53–55].

The TMD gluon densities in a proton calculated with fitted value of $b_g(0)$ and c_g are shown in Figs. 3 and 4 as functions of the proton's longitudinal momentum fraction x and gluon transverse momentum $\mathbf{k}_T^2$ for different values of the hard scale μ^2. The shaded bands represent the uncertainties of our fitting procedure.[8] As one can see, these

[7] We will not consider the ATLAS data [56] on b-jet production since they refer to extremely large b-jet transverse momenta, where the effects of parton showers and/or hadronization corrections play an important role.

[8] We neglected here the uncertainties connected with the c_g value since they are small compared to the ones related to the fit of the $b_g(0)$ parameter.

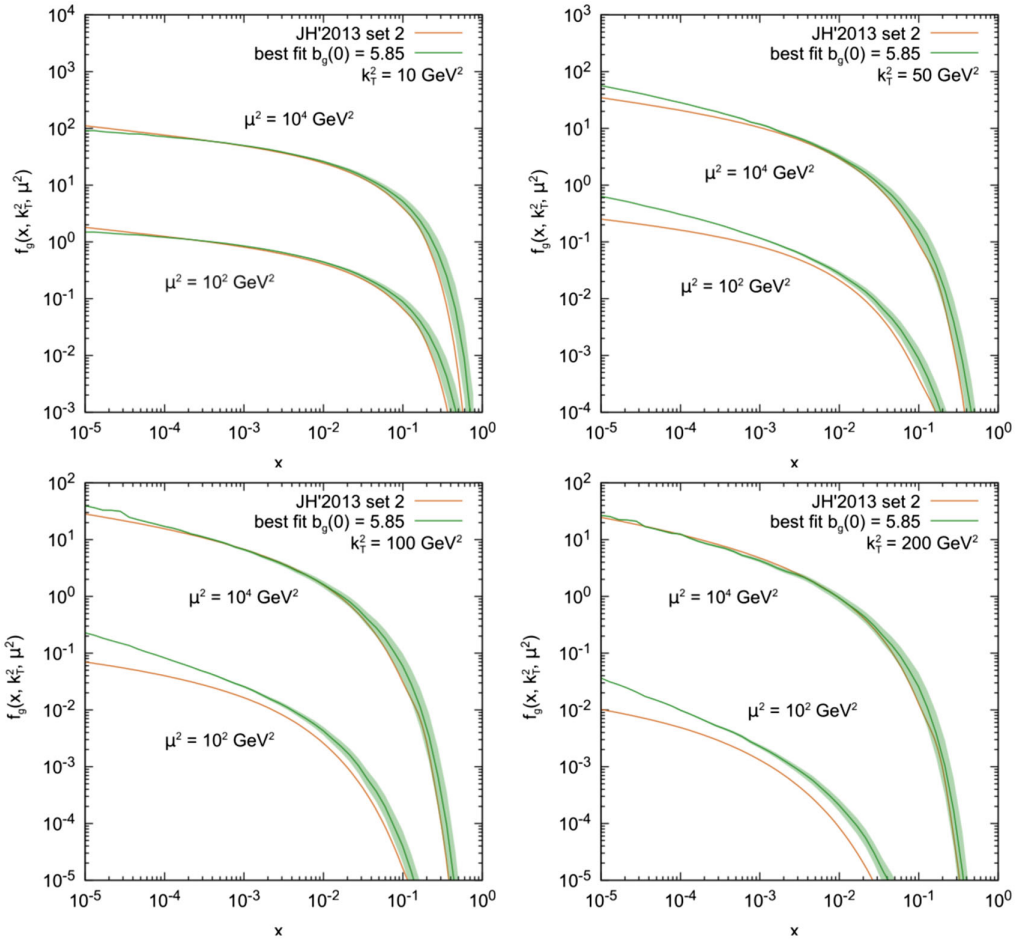

FIG. 3. The TMD gluon densities in a proton $f_g(x, \mathbf{k}_T^2, \mu^2)$ calculated as a function of the longitudinal momentum fraction x at different values of transverse momentum $\mathbf{k}_T^2$ and hard scale μ^2. Shaded bands represent the uncertainties of the $b_g(0)$ fitting procedure. The uncertainties connected with the fit of the c_g parameter are small and therefore not shown here. Note that the gluon densities calculated at $\mu^2 = 10^4$ GeV^2 are multiplied by a factor of 100.

uncertainties become important at $x \geq 10^{-1}$. For comparison, we also show the CCFM-evolved TMD gluon distributions from [15], namely, JH'2013 set 2, which is often used in the phenomenological applications. In contrast with our approach, the x dependence of the JH'2013 set 2 input has a general form given by (1) with parameters derived from the high-precision HERA data on the proton structure functions $F_2(x, Q^2)$ and $F_2^c(x, Q^2)$ at $x < 5 \times 10^{-3}$ and $Q^2 > 3.5$ GeV^2. We find that both of these gluon densities have a remarkably different x and $\mathbf{k}_T^2$ behavior, especially in the region of small $\mathbf{k}_T^2$; see Fig. 4. Some phenomenological consequences of the latter we demonstrate here.

So, the experimental data involved in our fit are compared with the obtained predictions in Figs. 5–11. The shaded bands represent the theoretical uncertainties of our calculations. For comparison, we also used here the JH'2013 set 2 gluon distribution. One can see that our fit leads to a good agreement with the experimental data practically for all considered observables. The HERA data on structure functions $F_2^c(x, Q^2)$, $F_2^c(x, Q^2)$ and reduced cross sections $\sigma_{\rm red}^c(x, Q^2)$, $\sigma_{\rm red}^b(x, Q^2)$ are reasonably well described by both considered TMD gluons within the uncertainties. However, we find that the JH'2013 set 2 gluon density provides a bit worse description of b-jet and/or Higgs boson production at the LHC, especially at low transverse momenta (see Figs. 5–7). The better agreement of these data achieved with the proposed TMD gluon density is an immediate consequence of using the physically motivated expression (24) for input distribution. In fact, at low transverse momenta, the relatively small gluon $\mathbf{k}_T^2$ are probed, where the difference between the considered gluon distributions becomes essential, as is shown in Fig. 4. Moreover, significant overestimation of the measured b-jet and especially the Higgs boson p_T spectra at low p_T obtained with the JH'2013 set 2 gluon leads to a notable difference in the absolute normalization of Higgs rapidity, decay photon scattering angle $\cos\theta^*$, invariant masses m_{12}, m_{34}, and other observables shown in Figs. 6 and 7. So, our calculations clearly demonstrate that the experimental data for the considered processes are strongly sensitive to the

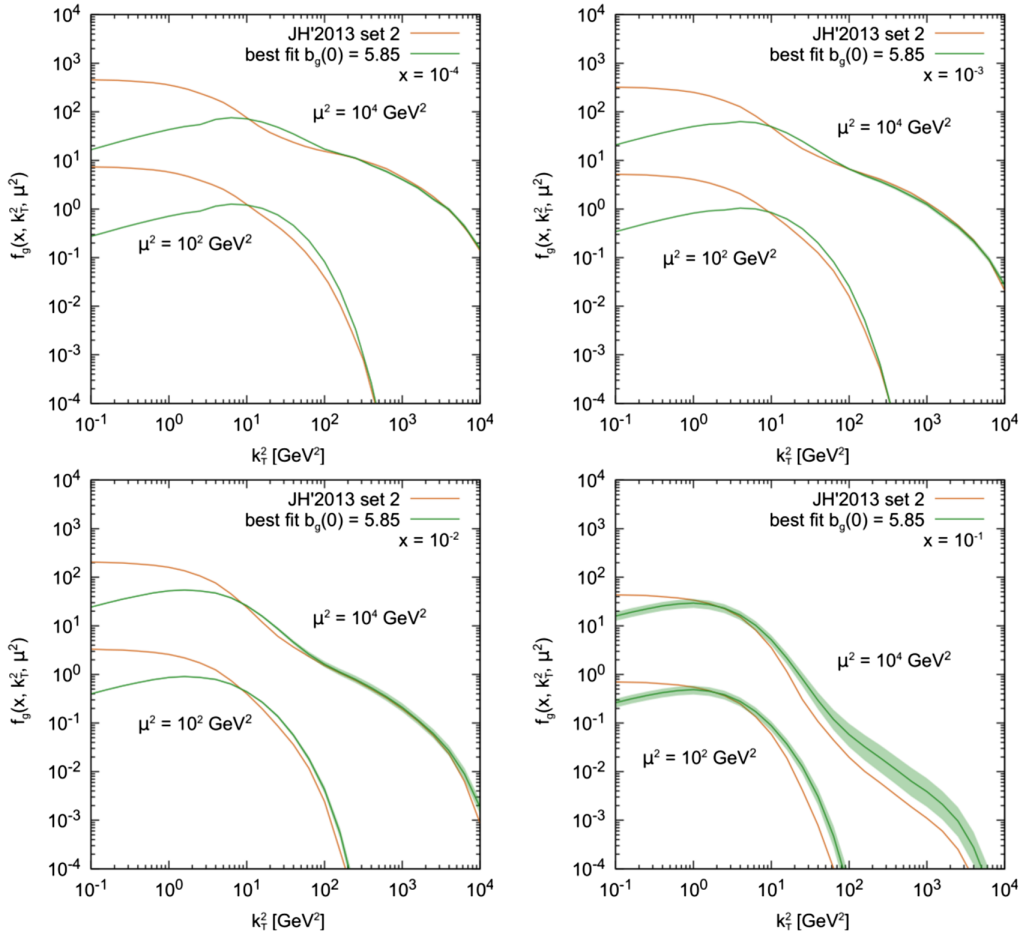

FIG. 4. The TMD gluon densities in a proton $f_g(x, \mathbf{k}_T^2, \mu^2)$ calculated as a function of the transverse momentum $\mathbf{k}_T^2$ at different values of the longitudinal momentum fraction x and hard scale μ^2. Shaded bands represent the uncertainties of the $b_g(0)$ fitting procedure. The uncertainties connected with the fit of the c_g parameter are small and therefore not shown here. Note that the gluon densities calculated at $\mu^2 = 10^4$ GeV^2 are multiplied by a factor of 100.

TMD gluon distribution in the proton and can be used to constrain the latter. Of course, future more precise measurements could be very useful and important to reduce the uncertainties in the determination of the phenomenological parameters from the data.

We performed here a step toward the global analysis of collider data in the k_T-factorization approach. The obtained TMD gluon density is already available for the community. It is implemented in the Monte Carlo event generator PEGASUS. Moreover, it is included in TMDLIB package, which is used by the CASCADE and KATIE Monte Carlo generators.

IV. CONCLUSION

We have proposed a new analytical expression for the TMD gluon density in the proton valid in a soft kinematical region. Using the modified quark-quark gluon string model, where the gluonic state and nonzero transverse momentum of partons inside the proton are taken into account, we have obtained some corresponding phenomenological parameters from the best description of LHC data on charged hadron (pion and kaon) spectra produced in pp collisions at low transverse momenta $p_T \simeq 1$ GeV. We have shown that the new suggested TMD gluon distribution incorporates saturation effects for the dipole cross section at a scale lower than the prediction of GBW model. Then, treating the obtained TMD gluon distribution as the initial condition for the subsequent noncollinear QCD evolution, we have extended it to the whole kinematical region using the CCFM equation. Several parameters important at moderate and large x have been fitted from the LHC data on inclusive b-jet and Higgs boson production as well as latest HERA data on proton structure functions $F_2^c(x, Q^2)$ and $F_2^b(x, Q^2)$ and reduced cross sections $\sigma_{\rm red}^c(x, Q^2)$ and $\sigma_{\rm red}^b(x, Q^2)$. Our fit leads to a simultaneous description of all these processes with good $\chi^2/\text{d.o.f.} = 2.2$. The obtained TMD gluon distribution in a proton is available for public usage and is implemented in the popular TMDLIB package and Monte Carlo event generator PEGASUS.

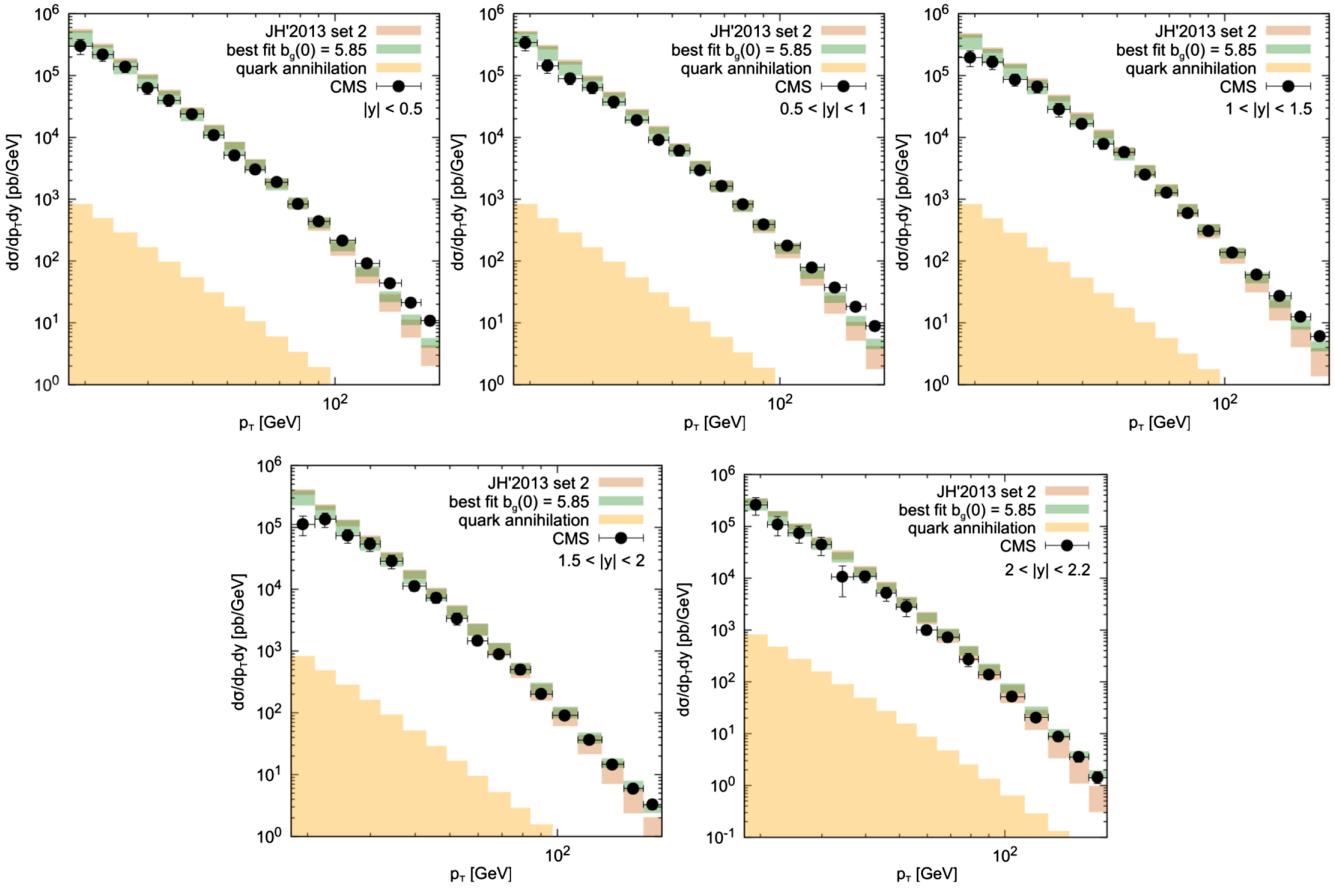

FIG. 5. Transverse momentum distributions of inclusive b-jets produced in pp collisions at $\sqrt{s} = 7$ TeV at different rapidities calculated using the CCFM-evolved TMD gluon density (24) with fitted value $b_g(0) = 5.85$. Predictions obtained with the JH'2013 set 2 gluon are shown for comparison. Shaded bands represent the estimation of theoretical uncertainties of our calculations. Kinematical cuts are described in the text. Experimental data are from CMS [52].

ACKNOWLEDGMENTS

We thank S. P. Baranov, A. A. Prokhorov, H. Jung, S. M. Turchikhin, and S. Taheri Monfared for their important comments and remarks. The studies described in Sec. II were supported by the Russian Science Foundation under Grant No. 22-22-00387. The updated release of the Monte Carlo generator PEGASUS (version 1.07.01) was supported by the Russian Science Foundation, Grant No. 22-22-00119.

APPENDIX A

In the conventional QGSM framework (neglecting the transverse momentum dependence), the quark and diquark distribution functions in a proton $f_a(x)$, where $a = u$, d, ud, or uu, were calculated [29,30]. They read

$$f_u(x) = C_u^p x^{-1/2}(1-x)^{3/2},$$
$$f_d(x) = C_d^p x^{-1/2}(1-x)^{5/2}, \tag{A1}$$
$$f_{ud}(x) = C_{ud}^p (1-x)^{-1/2} x^{3/2},$$
$$f_{uu}(x) = C_{ud}^p (1-x)^{-1/2} x^{5/2}. \tag{A2}$$

Here, the overall normalization factors are given by

$$C_u^p = C_{ud}^p = \frac{\Gamma(2-1/2+3/2)}{\Gamma(1-1/2)\Gamma(1+3/2)} = 1/1.1781, \tag{A3}$$

$$C_d^p = C_{uu}^p = \frac{\Gamma(2-1/2+5/2)}{\Gamma(1-1/2)\Gamma(1+5/2)} = 1/1.01859. \tag{A4}$$

In the modified QGSM, where the gluonic state in the proton and partonic transverse momentum are taken into account, the TMD quark and diquark densities can be written as

$$f_a(x, \mathbf{k}_T^2) = c_a f_a(x) g_a(\mathbf{k}_T^2), \qquad g_a(\mathbf{k}_T^2) = \frac{B_a^2}{2\pi} e^{-B_a|\mathbf{k}_T|}, \tag{A5}$$

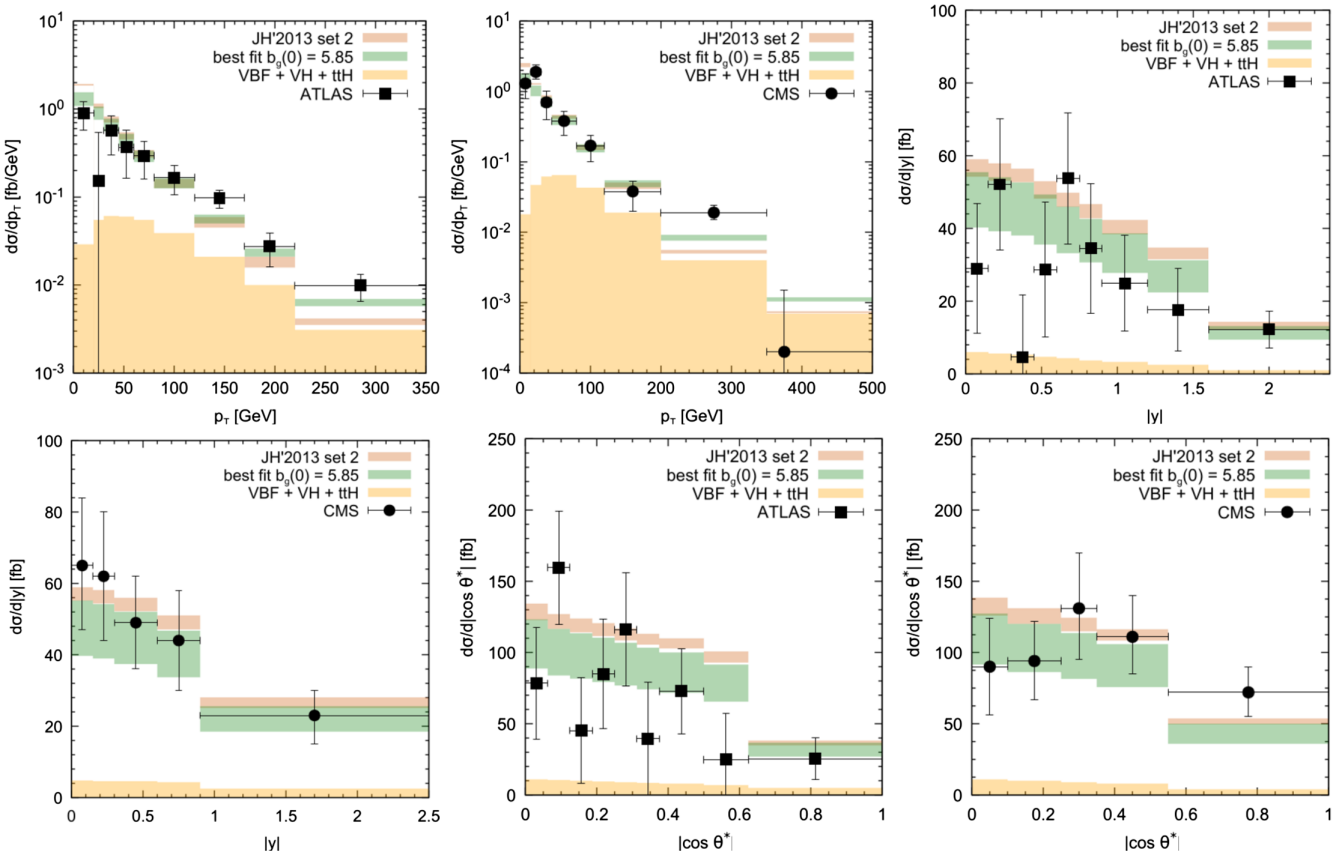

FIG. 6. Differential cross sections of inclusive Higgs boson production at $\sqrt{s} = 13$ TeV (in the diphoton decay mode) calculated as functions of the diphoton transverse momentum p_T, rapidity y, and photon helicity angle $|\cos\theta^*|$ (in the Collins-Soper frame). Notation of all histograms is the same as in Fig. 5. Kinematical cuts are described in the text. Experimental data are from ATLAS [53] and CMS [55].

where $B_q = B_{qq} = 5$ GeV^{-1}. The normalization factors c_a (which are about $1/2$) can be included to restore QCD quark-gluon sum rules.

Here we list the analytical expressions for the quark, diquark, and gluon fragmentation functions used in our calculations. These expressions were obtained in the QGSM at the LO [41]. So, for the gluons we have

$$G_{g\to h}(z,|\mathbf{p}_T|) = 2G_{g\to\pi}(z)I^g_\pi(|\mathbf{p}_T|) + 2G_{g\to K}(z)I^g_K(|\mathbf{p}_T|), \tag{A6}$$

where the coefficients 2 come from the following relations:

$$G_{g\to\pi^+}(z) = G_{g\to\pi^-}(z), \qquad G_{g\to K^+}(z) = G_{g\to K^-}(z). \tag{A7}$$

The parametrizations of $G_{g\to\pi}(z)$ and $G_{g\to K}(z)$ are the following:

$$G_{g\to\pi}(z) = 6.57z^{0.54}(1-z)^{3.01}, \tag{A8}$$

$$G_{g\to K}(z) = 0.37z^{0.79}(1-z)^{3.07}, \tag{A9}$$

and the functions $I^g_\pi(|\mathbf{p}_T|)$ and $I^g_K(|\mathbf{p}_T|)$ read

$$I^g_\pi(|\mathbf{p}_T|) = I^g_K(|\mathbf{p}_T|) = I^g_h(|\mathbf{p}_T|) = \frac{(B^g_{f_h})^2}{2\pi} e^{-B^g_{f_h}|\mathbf{p}_T|}, \tag{A10}$$

with $B^g_{f_h} = B^g_{f_\pi} = B^g_{f_K} = 4.5$ GeV^{-1}. For the quark fragmentation functions we have

$$G_{u\to\pi^+}(z,|\mathbf{p}_T|) = [a_0(1-z) + a_0(1-z)^2]I^q_\pi(|\mathbf{p}_T|), \tag{A11}$$

$$G_{d\to\pi^+}(z,|\mathbf{p}_T|) = (1-z)G_{u\to\pi^+}(z)I^q_\pi(|\mathbf{p}_T|), \tag{A12}$$

$$G_{u\to K^+}(z,|\mathbf{p}_T|) = a_k(1-z)^{1/2}(1+a_{1K}z)I^q_K(|\mathbf{p}_T|), \tag{A13}$$

$$G_{u\to K^-}(z,|\mathbf{p}_T|) = a_k(1-z)^{3/2}I^q_K(|\mathbf{p}_T|), \tag{A14}$$

$$G_{d\to K^+}(z,|\mathbf{p}_T|) = G_{u\to K^-}(z)I^q_K(|\mathbf{p}_T|), \tag{A15}$$

$$G_{d\to K^-}(z,|\mathbf{p}_T|) = G_{u\to K^+}(z)I^q_K(|\mathbf{p}_T|). \tag{A16}$$

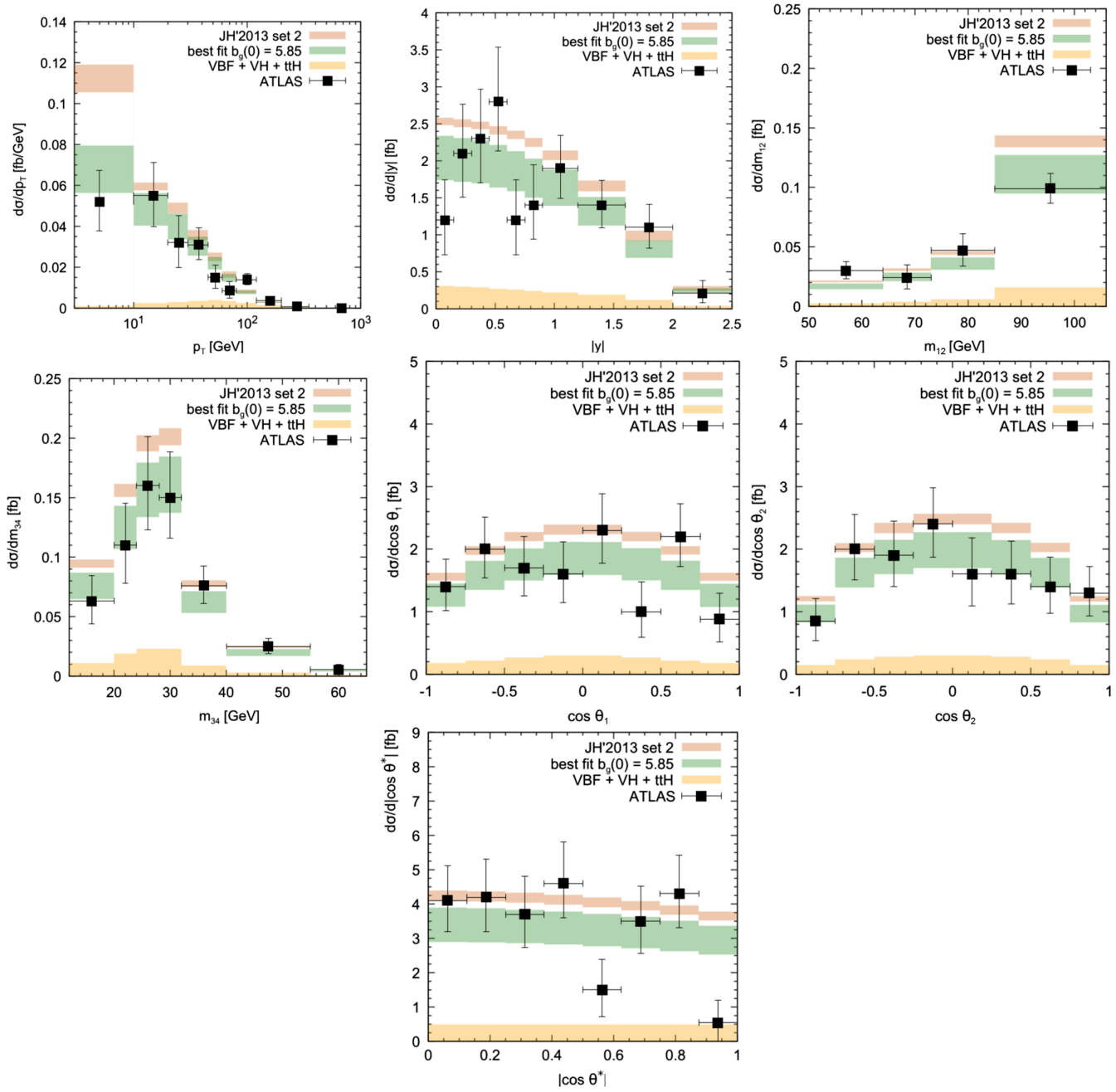

FIG. 7. Differential cross sections of inclusive Higgs boson production at $\sqrt{s} = 13$ TeV (in the $H \to ZZ^* \to 4l$ decay mode) calculated as functions of the Higgs transverse momentum p_T, rapidity y, leading and subleading lepton pair invariant masses m_{12} and m_{34}, leading lepton pair scattering angle $|\cos\theta^*|$ (in the Collins-Soper frame), and first and second antilepton production angles $\cos\theta_1$ and $\cos\theta_2$. The notation of all histograms is the same as in Fig. 5. The kinematical cuts are described in the text. The experimental data are from ATLAS [54].

The analytical forms for $I^q_\pi(|\mathbf{p}_T|)$ and $I^q_K(|\mathbf{p}_T|)$ are the same as for $I^g_\pi(|\mathbf{p}_T|)$, $I^g_K(|\mathbf{p}_T|)$, but the slopes are $B^q_{f_\pi} = B^q_{f_K} = 7\ \mathrm{GeV}^{-1}$. The other parameters are $a_0 = 0.65$, $a_k = 0.075$, and $a_{1K} = 2$. Finally, for the diquarks one can write

$$G_{uu\to\pi^+}(z,|\mathbf{p}_T|) = a_0(1-z)^2 I^{qq}_\pi(|\mathbf{p}_T|), \quad \text{(A17)}$$

$$G_{ud\to\pi^+}(z,|\mathbf{p}_T|) = a_0(1+(1-z)^2)(1-z)^2 I^{qq}_\pi(|\mathbf{p}_T|), \quad \text{(A18)}$$

$$G_{uu\to K^+}(z,|\mathbf{p}_T|) = a_k(1-z)^{5/2}(1+a_{2K}z) I^{qq}_K(|\mathbf{p}_T|), \quad \text{(A19)}$$

$$G_{uu\to K^-}(z,|\mathbf{p}_T|) = a_k(1-z)^{7/2} I^{qq}_K(|\mathbf{p}_T|), \quad \text{(A20)}$$

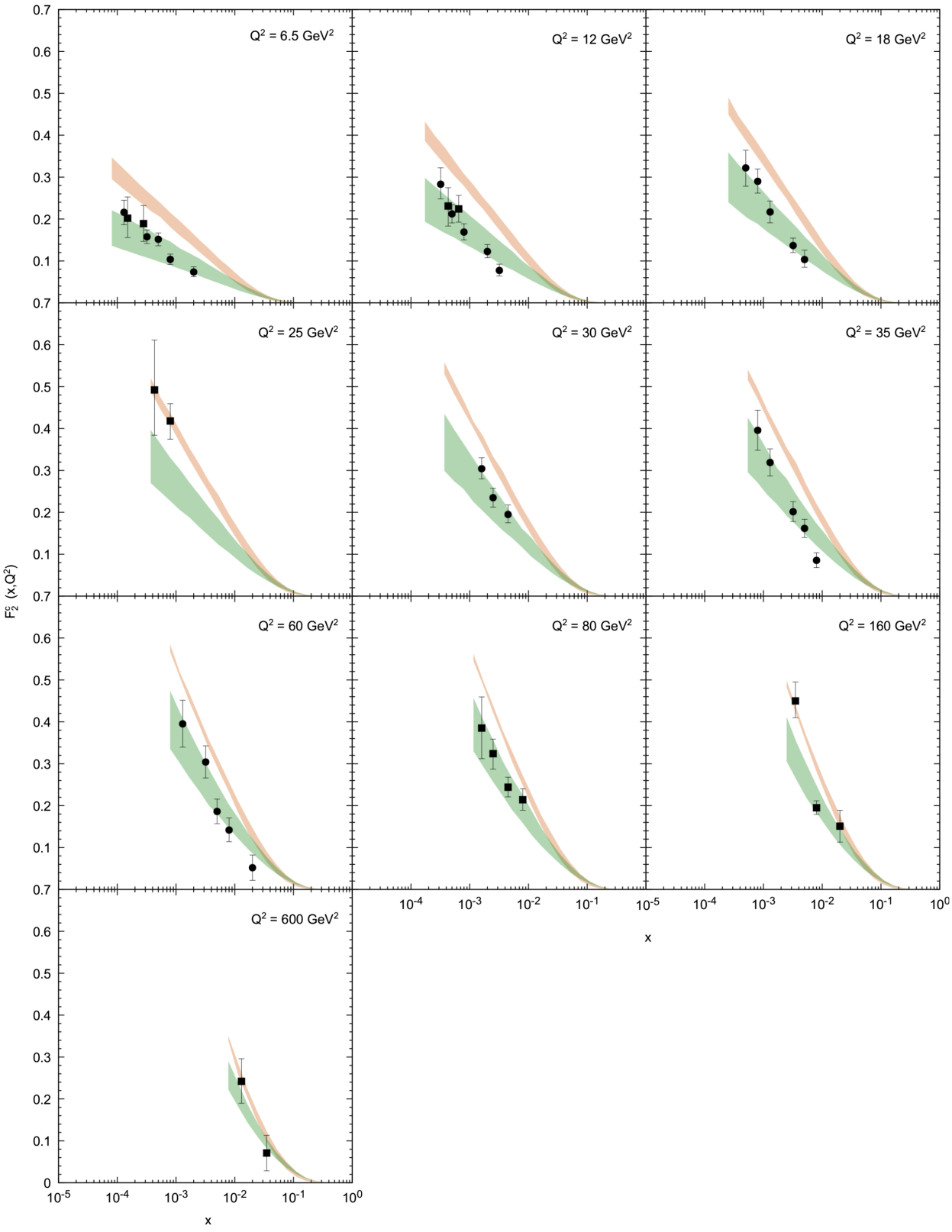

FIG. 8. Structure functions $F_2^c(x, Q^2)$ measured at different scales calculated using the CCFM-evolved TMD gluon density (24) with fitted value $b_g(0) = 5.85$. Predictions obtained with the JH'2013 set 2 gluon are shown for comparison. Shaded bands represent the estimation of theoretical uncertainties of our calculations. Experimental data are from ZEUS and H1 [57–59].

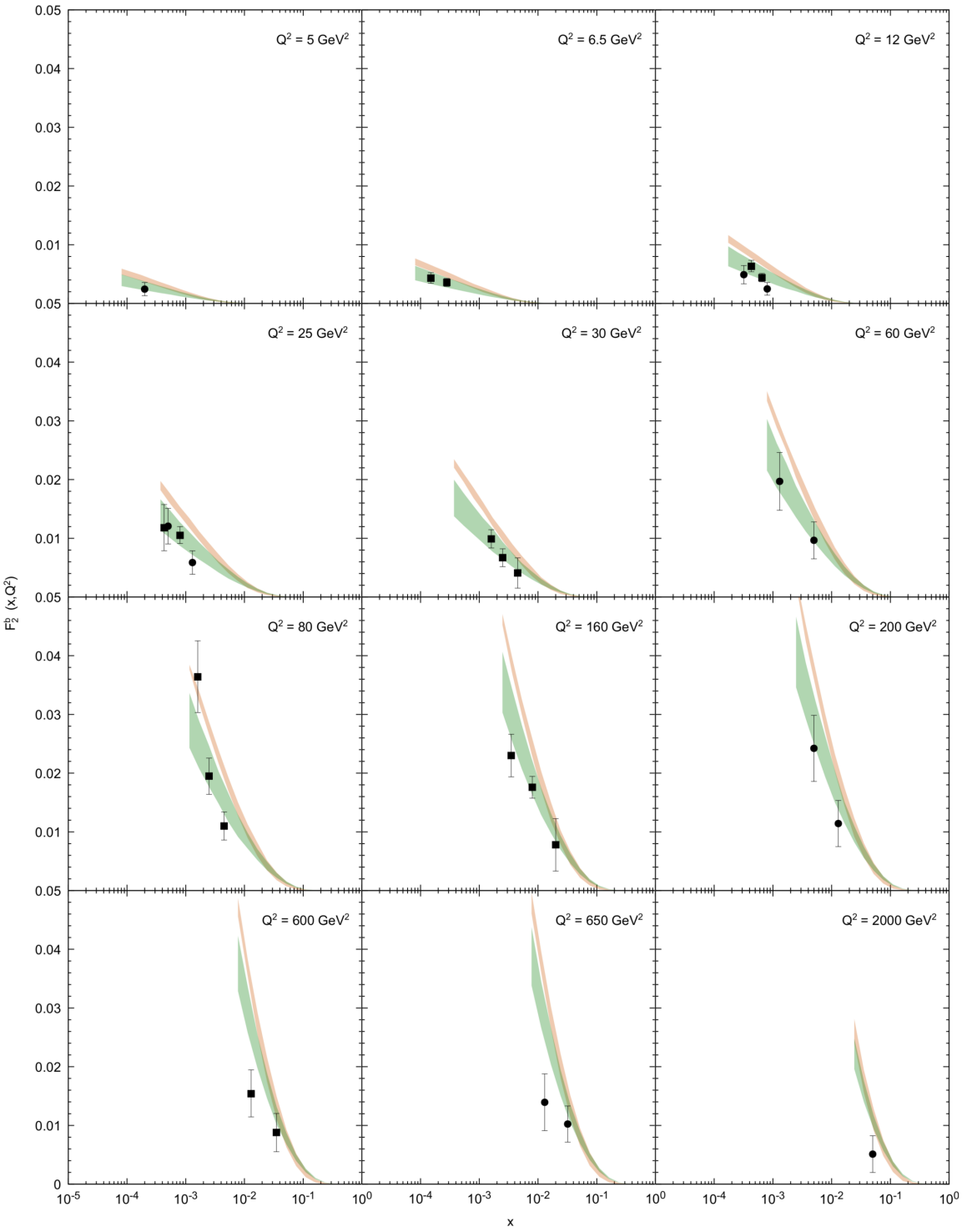

FIG. 9. Structure functions $F_2^b(x, Q^2)$ measured at different scales calculated using the CCFM-evolved TMD gluon density (24) with fitted value $b_g(0) = 5.85$. Predictions obtained with the JH'2013 set 2 gluon are shown for comparison. Shaded bands represent the estimation of theoretical uncertainties of our calculations. Experimental data are from ZEUS and H1 [57,59].

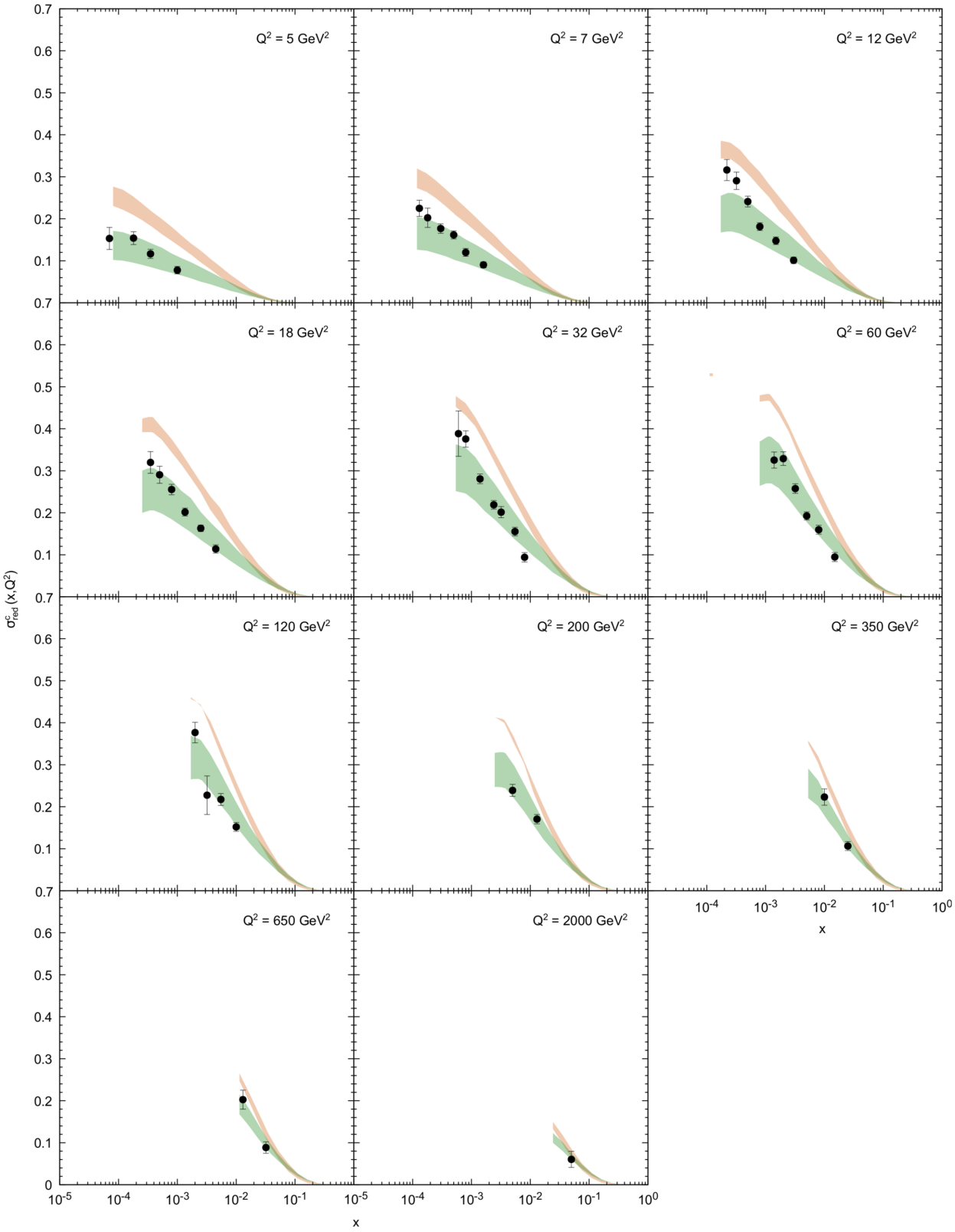

FIG. 10. Reduced cross sections $\sigma^c_{\rm red}(x, Q^2)$ measured at different scales calculated using the CCFM-evolved TMD gluon density (24) with fitted value $b_g(0) = 5.85$. Predictions obtained with the JH'2013 set 2 gluon are shown for comparison. Shaded bands represent the estimation of theoretical uncertainties of our calculations. Experimental data are from ZEUS and H1 [60].

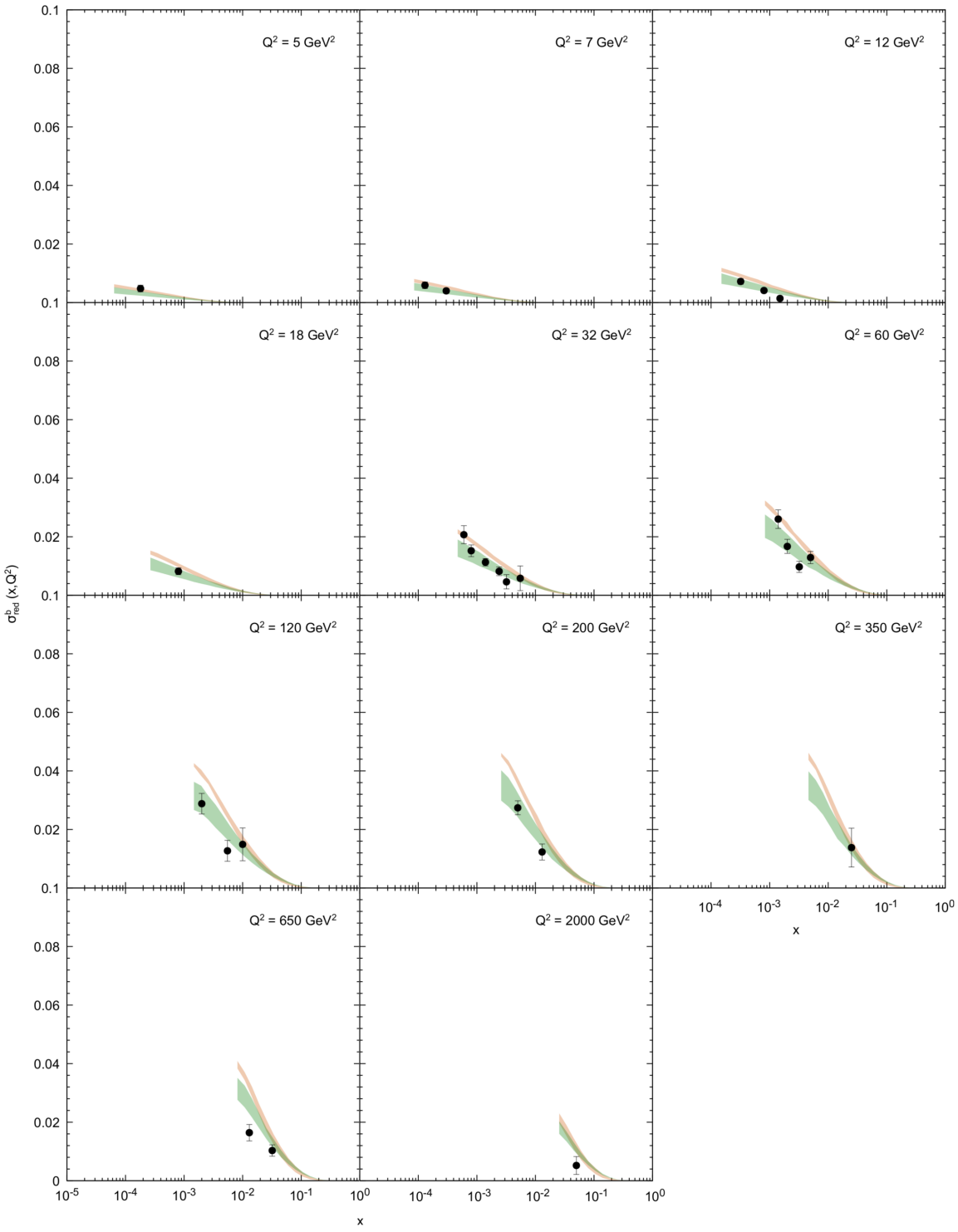

FIG. 11. Structure functions $\sigma^b_{\mathrm{red}}(x, Q^2)$ measured at different scales calculated using the CCFM-evolved TMD gluon density (24) with fitted value $b_g(0) = 5.85$. Predictions obtained with the JH'2013 set 2 gluon are shown for comparison. Shaded bands represent the estimation of theoretical uncertainties of our calculations. Experimental data are from ZEUS and H1 [60].

$$G_{ud\to K^+}(z,|\mathbf{p}_T|)=\frac{a_k}{2}(1-z)^{5/2}(1+a_{2K}z+(1-z)^2)I_K^{qq}(|\mathbf{p}_T|), \tag{A21}$$

$$G_{ud\to K^-}(z,|\mathbf{p}_T|)=\frac{a_k}{2}(1-z)^{7/2}(1+(1-z)^2)I_K^{qq}(|\mathbf{p}_T|), \tag{A22}$$

where $I_{\pi,K}^{qq}(|\mathbf{p}_T|)=I_{\pi,K}^{q}(|\mathbf{p}_T|)$ and $a_{2K}=5$.

APPENDIX B

Here we present some details of our calculation of charged hadron spectra at low p_T. The functions Φ_a involved in (9) and (10) can be presented in the following way:

$$\Phi_a(x_\pm,p_T)=\int_{x_\pm}^{1}dx_1\int_0^\infty d\mathbf{k}_{1T}^2\int_0^{2\pi}d\varphi_1\int_{x_\pm}^{1-x_1}dx_2\int_0^\infty d\mathbf{k}_{2T}^2\int_0^{2\pi}d\phi_2\tilde{F}_a(x_1,x_2,\mathbf{k}_{1T}^2,\mathbf{k}_{2T}^2)G_{a\to h}(z,|\mathbf{p}_T-z\mathbf{k}_{1T}|), \tag{B1}$$

where $a=q$, qq, or g and $z=x_\pm/x_1$. The kernels $\tilde{F}_a(x_1,x_2,\mathbf{k}_{1T}^2,\mathbf{k}_{2T}^2)$ are

$$\tilde{F}_q^g(x_1,x_2,\mathbf{k}_{1T}^2,\mathbf{k}_{2T}^2)=f_q(x_1)g_q(\mathbf{k}_{1T}^2)f_{qq}(1-x_1-x_2)g_{qq}(|\mathbf{k}_{1T}+\mathbf{k}_{2T}|^2)f_g(x_2,\mathbf{k}_{2T}^2), \tag{B2}$$

$$\tilde{F}_{qq}^g(x_1,x_2,\mathbf{k}_{1T}^2,\mathbf{k}_{2T}^2)=f_{qq}(x_1)g_{qq}(\mathbf{k}_{1T}^2)f_q(1-x_1-x_2)g_q(|\mathbf{k}_{1T}+\mathbf{k}_{2T}|^2)f_g(x_2,\mathbf{k}_{2T}^2), \tag{B3}$$

$$\tilde{F}_g(x_1,x_2,\mathbf{k}_{1T}^2,\mathbf{k}_{2T}^2)=f_g(x_1,\mathbf{k}_{1T}^2)f_q(1-x_1-x_2)g_q(|\mathbf{k}_{1T}+\mathbf{k}_{2T}|^2)f_{qq}(x_2)g_{qq}(\mathbf{k}_{2T}^2). \tag{B4}$$

To simplify the integration in (B1), we perform a change of variables:

$$\begin{aligned}&x_1=t_0(1-x_\pm)+x_\pm, \qquad \mathbf{k}_{1T}^2=(1-t_1)/t_1, \qquad \varphi_1=2\pi t_2,\\ &x_2=t_3(1-x_1)=t_3(1-x_\pm)(1-t_0)+x_\pm, \qquad \mathbf{k}_{2T}^2=(1-t_4)/t_4, \qquad \varphi_2=2\pi t_5.\end{aligned} \tag{B5}$$

The integration on all t variables can now be performed in the range (0,1). The transition Jacobian reads

$$J(x_\pm,t_0,\ldots,t_5)=\frac{4\pi^2(1-x_\pm)(1-x_1(t_0))}{t_1^2t_4^2}=\frac{4\pi^2(1-x_\pm)^2(1-t_0)}{t_1^2t_4^2}. \tag{B6}$$

[1] V. N. Gribov and L. N. Lipatov, Sov. J. Nucl. Phys. **15**, 438 (1972); N. Lipatov, Sov. J. Nucl. Phys. **20**, 94 (1975); G. Altarelli and G. Parisi, Nucl. Phys. **B126**, 298 (1977); Yu. L. Dokshitzer, Sov. Phys. JETP **46**, 641 (1977).

[2] R. Angeles-Martinez *et al.*, Acta Phys. Pol. B **46**, 2501 (2015).

[3] E. A. Kuraev, L. N. Lipatov, and V. S. Fadin, Sov. Phys. JETP **44**, 443 (1976); E. A. Kuraev, L. N. Lipatov, and V. S. Fadin, Sov. Phys. JETP **45**, 199 (1977); I. I. Balitsky and L. N. Lipatov, Sov. J. Nucl. Phys. **28**, 822 (1978).

[4] M. Ciafaloni, Nucl. Phys. **B296**, 49 (1988); S. Catani, F. Fiorani, and G. Marchesini, Phys. Lett. B **234**, 339 (1990); S. Catani, F. Fiorani, and G. Marchesini, Nucl. Phys. **B336**, 18 (1990); G. Marchesini, Nucl. Phys. **B445**, 49 (1995).

[5] S. Catani, M. Ciafaloni, and F. Hautmann, Nucl. Phys. **B366**, 135 (1991); J. C. Collins and R. K. Ellis, Nucl. Phys. **B360**, 3 (1991).

[6] L. V. Gribov, E. M. Levin, and M. G. Ryskin, Phys. Rep. **100**, 1 (1983); E. M. Levin, M. G. Ryskin, Yu. M. Shabelsky, and A. G. Shuvaev, Sov. J. Nucl. Phys. **53**, 657 (1991).

[7] H. Jung, S. P. Baranov, A. Bermudez Martinez, L. I. Estevez Banos, F. Guzman, F. Hautmann, A. Lelek, J. Lidrych, A. V. Lipatov, M. A. Malyshev, M. Mendizabal, S. Taheri Monfared, A. M. van Kampen, Q. Wang, and H. Yang, Eur. Phys. J. C **81**, 425 (2021).

[8] A. van Hameren, Comput. Phys. Commun. **224**, 371 (2018).

[9] A. V. Lipatov, M. A. Malyshev, and S. P. Baranov, Eur. Phys. J. C **80**, 330 (2020).

[10] M. A. Kimber, A. D. Martin, and M. G. Ryskin, Phys. Rev. D **63**, 114027 (2001); A. D. Martin, M. G. Ryskin, and G. Watt, Eur. Phys. J. C **31**, 73 (2003).
[11] A. D. Martin, M. G. Ryskin, and G. Watt, Eur. Phys. J. C **66**, 163 (2010).
[12] I. Balitsky, Nucl. Phys. **B463**, 99 (1996); Y. V. Kovchegov, Phys. Rev. D **60**, 034008 (1999).
[13] L. V. Gribov, E. M. Levin, and M. G. Ryskin, Phys. Rep. **100**, 1 (1983).
[14] Yu. Shi, Sh.-Yi. Wei, and J. Zhou, arXiv:2211.07174.
[15] F. Hautmann and H. Jung, Nucl. Phys. **B883**, 1 (2014).
[16] F. Hautmann, H. Jung, A. Lelek, V. Radescu, and R. Zlebcik, Phys. Lett. B **772**, 446 (2017).
[17] F. Hautmann, H. Jung, A. Lelek, V. Radescu, and R. Zlebcik, J. High Energy Phys. 01 (2018) 070.
[18] N. A. Abdulov *et al.*, Eur. Phys. J. C **81**, 752 (2021).
[19] E. Avsar, Int. J. Mod. Phys. Conf. Ser. **04**, 74 (2011).
[20] S. M. Aybat and T. C. Rogers, Phys. Rev. D **83**, 114042 (2011).
[21] B. I. Ermolaev, M. Greco, and S. I. Troyan, Eur. Phys. J. C **71**, 1750 (2011); B. I. Ermolaev, M. Greco, and S. I. Troyan, Eur. Phys. J. C **72**, 1953 (2012).
[22] P. Kotko, K. Kutak, C. Marquet, E. Petreska, S. Sapeta, and A. van Hameren, J. High Energy Phys. 09 (2015) 106.
[23] A. A. Grinyuk, A. V. Lipatov, G. I. Lykasov, and N. P. Zotov, Phys. Rev. D **87**, 074017 (2013).
[24] A. V. Lipatov, G. I. Lykasov, and N. P. Zotov, Phys. Rev. D **89**, 014001 (2014).
[25] A. A. Grinyuk, A. V. Lipatov, G. I. Lykasov, and N. P. Zotov, Phys. Rev. D **93**, 014035 (2016).
[26] N. A. Abdulov, H. Jung, A. V. Lipatov, G. I. Lykasov, and M. A. Malyshev, Phys. Rev. D **98**, 054010 (2018).
[27] A. Bermudez Martinez, P. Connor, H. Jung, A. Lelek, R. Zlebcik, F. Hautmann, and V. Radescu, Phys. Rev. D **99**, 074008 (2019).
[28] V. Bertone, M. Botje, D. Britzger, S. Camarda, A. Cooper-Sarkar, F. Giuli, A. Glazov, A. Luszczak, F. Olness, R. Placakyte, V. Radescu, W. Slominski, and O. Zenaiev, *Proc. Sci.* DIS2017 (2018) 203 [arXiv:1709.01151].
[29] A. B. Kaidalov, Z. Phys. C **12**, 63 (1982); A. B. Kaidalov, Surv. High Energy Phys. **13**, 265 (1999); A. B. Kaidalov and O. I. Piskunova, Z. Phys. C **30**, 145 (1986).
[30] G. I. Lykasov and M. N. Sergeenko, Z. Phys. C **52**, 635 (1991); **56**, 697 (1992); **70**, 455 (1996).
[31] V. A. Bednyakov, G. I. Lykasov, and V. V. Lyubushkin, Europhys. Lett. **92**, 31001 (2010).
[32] V. A. Bednyakov, A. A. Grinyuk, G. I. Lykasov, and M. Poghosyan, Int. J. Mod. Phys. A **27**, 1250042 (2012).
[33] K. Golec-Biernat and M. Wüsthoff, Phys. Rev. D **59**, 014017 (1998).
[34] K. Golec-Biernat and M. Wüsthoff, Phys. Rev. D **60**, 114023 (1999).
[35] Yu. V. Kovchegov, Phys. Rev. D **61**, 074018 (2000).
[36] A. Capella, U. Sukhatme, C. J. Tan, and J. Tran Thanh Van, Phys. Rev. D **36**, 109 (1987).
[37] V. Abramovsky, V. N. Gribov, and O. Kancheli, Sov. J. Nucl. Phys. **18**, 308 (1973).
[38] ZEUS Collaboration, Phys. Lett. B **487**, 53 (2000).
[39] ZEUS Collaboration, Eur. Phys. J. C **21**, 443 (2001).
[40] S. I. Sinegovsky and M. N. Sorokovikov, Eur. Phys. J. C **80**, 34 (2020).
[41] J. Binnewies, B. A. Kniehl, and G. Kramer, Phys. Rev. D **52**, 4947 (1995).
[42] N. Cartiglia, arXiv:1305.6131.
[43] I. M. Dremin, Particles **2**, 57 (2019).
[44] G. P. Lepage, J. Comput. Phys. **27**, 192 (1978).
[45] ATLAS Collaboration, New J. Phys. **13**, 053033 (2011).
[46] CMS Collaboration, Phys. Rev. Lett. **105**, 022002 (2010).
[47] ATLAS Collaboration, Eur. Phys. J. C **76**, 502 (2016).
[48] A. V. Kotikov, A. V. Lipatov, B. G. Shaikhatdenov, and P. Zhang, J. High Energy Phys. 02 (2020) 028.
[49] A. V. Kotikov, A. V. Lipatov, and P. Zhang, Phys. Rev. D **104**, 054042 (2021).
[50] A. V. Kotikov, B. G. Shaikhatdenov, and P. Zhang, Phys. Rev. D **96**, 114002 (2017).
[51] F. Hautmann, H. Jung, and S. Taheri Monfared, Eur. Phys. J. C **74**, 3082 (2014).
[52] CMS Collaboration, J. High Energy Phys. 04 (2012) 084.
[53] ATLAS Collaboration, Phys. Rev. D **98**, 052005 (2018).
[54] ATLAS Collaboration, Eur. Phys. J. C **80**, 942 (2020).
[55] CMS Collaboration, J. High Energy Phys. 01 (2019) 183.
[56] ATLAS Collaboration, Eur. Phys. J. C **71**, 1846 (2011).
[57] ZEUS Collaboration, J. High Energy Phys. 09 (2014) 127.
[58] H1 Collaboration, Eur. Phys. J. C **71**, 1769 (2011).
[59] H1 Collaboration, Eur. Phys. J. C **65**, 89 (2010).
[60] ZEUS and H1 Collaborations, Eur. Phys. J. C **78**, 473 (2018).
[61] H. Jung, M. Krämer, A. V. Lipatov, and N. P. Zotov, J. High Energy Phys. 01 (2011) 085; Phys. Rev. D **85**, 034035 (2012).
[62] A. V. Lipatov, M. A. Malyshev, and N. P. Zotov, Phys. Lett. B **735**, 79 (2014); N. A. Abdulov, A. V. Lipatov, and M. A. Malyshev, Phys. Rev. D **97**, 054017 (2018).
[63] A. V. Kotikov, A. V. Lipatov, G. Parente, and N. P. Zotov, Eur. Phys. J. C **26**, 51 (2002).